Measurement of temperature distributions across laser-heated samples by multispectral imaging radiometry

Andrew J. Campbell

Department of Geology, University of Maryland, College Park, MD 20742

(Submitted to *Rev. Sci. Instrum.*, 8 September 2007; Revised 27 November 2007; Accepted 3 December 2007)

Two-dimensional temperature mapping of laser-heated diamond anvil cell samples is performed by processing a set of four simultaneous images of the sample, each obtained at a narrow spectral range in the visible to near-infrared. The images are correlated spatially, and each set of four points is fit to the Planck radiation function to determine the temperature and the emissivity of the sample, using the gray body approximation. The method is tested by measuring the melting point of Pt at 1 bar, and measuring laser-heated Fe at 20 GPa in the diamond anvil cell. The accuracy and precision are shown to compare well to standard spectroradiometry, and the effect of imaging resolution on the measured distribution is evaluated. The principal advantages of the method are: 1) the temperature and emissivity of the sample are mapped in two dimensions; 2) chromatic aberrations are practically eliminated by independent focussing of each spectral band; and 3) all of the spectral images are obtained simultaneously, allowing temporal variations to be studied. This method of measuring temperature distributions can be generalized to other hot objects besides laser heated spots.

INTRODUCTION

Proper characterization of material properties and chemical reactions under high pressure, high temperature conditions requires that the pressure, temperature conditions, and their gradients, be accurately and precisely known. Understanding the nature of these thermodynamic gradients has always been one of the most significant challenges facing high-pressure experimentation. In general, technical considerations require that as the pressure and temperature increase, the gradients in these quantities also increase. A good example of this principle is the laser-heated diamond anvil cell, in which typical sample dimensions are on the 10^1 micron scale, and the temperature gradients can reach ~10^2 K/μm. The diamond cell has become the instrument of choice for obtaining high pressures (> 25 GPa) under static conditions, because of its simplicity of use, robustness of design, and the optical access afforded by the diamond anvils. Furthermore, to obtain the simultaneous high-pressure, high-temperature studies that are essential to geophysics and geochemistry, laser heating has emerged as the dominant method of attaining temperatures above 1500 K in diamond cell samples. Temperatures in laser heating are usually measured using spectroradiometry [1].

A significant drawback to the laser heating method is the unavoidable, strong temperature gradient. Typical laser-heated spot diameters are 25-50 μm, even with 50-100 W lasers, because the high thermal conductance of the diamond anvils requires very high power densities on the sample surface. Several strategies are commonly used to address this problem. One is simply to acknowledge the large uncertainty in temperature; many experiments (for example, synthesis of high pressure phases) are designed such that

they require only the the temperature be high, not that it be precisely known. Obviously this approach is unsatisfactory for many applications. Another strategy is to measure only temperature in one area (usually the center), and to analyze the sample only in this region. This can be a satisfactory approach in some cases, for example synchrotron x-ray diffraction experiments in which the probe beam (x-ray) is focussed to a size (perhaps 5 μm) that is much smaller than the laser-heated spot, and comparable to the area over which the temperature is measured. Other applications should require that the actual gradient in temperature be known; however, these gradients are much less commonly measured.

Early efforts to quantify the temperature of the laser heated spot involved measuring a series of slit measurements across the sample, and inverting for the radial gradient using Abel transforms of the measured intensities [1]. Later, pinhole apertures were translated to measure the temperature at a series of points across the sample [2, 3]. One of the drawbacks of these methods was that the gradient was measured over several minutes rather than simultaneously. With the advent of imaging spectrographs, the pinhole method evolved into simultaneous measurements of temperature across the diameter of the spot; the spectrograph entrance slit selected a strip of image centered on the hot spot, and each row of pixels on the CCD detector ideally represented a different point along the strip [4,5]. Related approaches used an imaging spectrometer with multiple input fibers [6] or with no entrance slit, combined with an Abel transform to determine the gradient [7,8]. These imaging methods require great care because of the many difficult alignment issues and the limitations to the imaging capability of the spectrographs [5,9].

Ultimately all of these gradient measurement methods have two significant weaknesses. One is the fact that they require aperturing the broadband thermal emission image; because of this, chromatic aberrations in the optical system can introduce serious errors in the measurement [4,5,10]. This was partly the basis for extensive debate in the literature over early applications of laser heating at high pressures [7,11,12]. Careful design, alignment and calibration can overcome much of the chromatic effect, but the diamond anvils will always introduce some uncertainty if small apertures are used [4,13]. The second weakness of early thermal gradient measurements is that they only determine temperature along a cross-section of the sample, and that cross-section is chosen before the experiment takes place. If the sample behaves ideally, with a radially symmetric temperature distribution, then a single radial profile is adequate. However, real laser heated diamond cell samples frequently absorb the sample asymmetrically because of variations in insulator thickness, sample surface conditions, etc., and a 2-dimensional T measurement is required for accurate description of the experimental conditions.

In this paper I describe a method of temperature measurement that overcomes these two limitations to a large degree. The strategy is to trade off spectoradiometric precision for 2-dimensional coverage; instead of measuring ~1000 wavelengths at a single point or small number of points, the method described here involves 2-D image collection at only a few (4 or more) spectral bands. The reduction in radiometric precision is acceptable, because in standard spectroradiometric measurement of laser-heated diamond cell samples the precision in fitting to the Planck function (~few K) greatly exceeds the demonstrated reliability of the technique (~50-100 K) [4].

The use of only a small number of spectral bands, rather than a heavily sampled spectrum, to make temperature measurements of high pressure samples has previously been applied in shock wave experiments (e.g., [14-16]). In that application, only a few (4 to 6) spectral bands are measured because each spectral measurement must be highly time-resolved, so a separate photodiode detector is devoted to each band. In the present application, an analogous trade-off is made, except here the purpose is spatial resolution in the temperature measurement, not time resolution.

Recently Kavner and Nugent [17] have taken the important step of recording the laser heated spot with a high dynamic range CCD camera to evaluate thermal gradients. The present work advances that technology by introducing the simultaneous measurement of several spectral bands, instead of only one at a time. In addition, unlike all earlier techniques, the method reported here provides for independent focussing of each spectral band, bypassing the chromatic aberrations that have plagued temperature measurements of laser heated spots.

EXPERIMENTS

Two types of samples were analyzed in this study, to evaluate the performance of the multispectral imaging radiometry system described below. The first was Pt foil at 1 bar, to gauge the accuracy and precision of the technique by comparing the measured melting temperature of Pt with the known value of 2045 K. The second sample was Fe at 20 GPa in a diamond anvil cell, to demonstrate the performance of the system in the

intended application of measuring T distributions across small (~30 μm) laser heated spots on high-pressure samples.

Sample preparation

The Pt foil was mounted on an Al block and held into place with machine screws, and then laser heated in air. The partial pressure of oxygen in air is insufficient to oxidize Pt at its melting point. Thin samples of Fe were prepared by compressing Fe powder into a foil in a diamond cell. A thin flake of this foil, approximately 5 μm thick and 60 μm in diameter, was then loaded into a symmetric-type diamond anvil cell, surrounded by NaCl, which acted as a pressure medium and insulator from the diamond anvils. The sample assembly was dried at 90 ˚C in an oven for 1 hour before closing the sample chamber. The sample was then compressed to 20 GPa, based on the ruby fluorescence pressure standard [18].

Optical systems

The laser heating system is diagrammed in Figure 1. The heating laser was a Yb-doped fiber laser, rated for 50 W of linearly polarized CW output at 1064 nm (IPG Photonics, Inc., model YLR-50-1064-LP). The laser was focussed into the diamond anvil cell using objective lens L1, which is an infinity-corrected 5X lens that is optimized for the near infrared and has a working distance of 37.5 mm. The divergence of this laser beam is small (< 0.5 mrad), which would produce an unnecessarily small laser heated spot using only the objective lens L1, so additional divergence was introduced into the beam by lenses L2 and L3 (Figure 1) to produce a laser spot size of ~30 μm on a

diamond anvil cell sample. The laser spot size can be adjusted by changing the distance between lenses L2 and L3. The laser light was aligned with the optical path of the microscope by mirror M1 and the sample was viewed using tube lens L4 and camera C1 (Figure 1). Filters F1 and F2 restrict viewing of the sample to the 600-950 nm band, which is similar to the wavelengths for which the temperature system is designed. Thermal emission from the laser heated spot was deflected from the microscope to the imaging radiometry system, and also to the standard spectroradiometry system, using pellicle beamsplitters BS1.

The imaging radiometry system is illustrated in Figure 2. The principle of this system is that it splits the image of the laser heated spot four ways, and each of these images is then filtered to allow only a narrow wavelength bandpass. The four separate images are then focussed independently onto the CCD camera C2. Before entering the system, the light is filtered to remove scattering from the 1064 nm laser and also visible wavelengths shorter than 600 nm. The tube lens (L5) has a nominal focal length of 500 mm, which produces nominally 12.5X magnification when used with objective lens L1. A series of cube beamsplitters BS2 produces four separate light paths, each of which reflect off of the mirrors M3 and then pass back through the beamsplitters BS2. Translation of the M3 mirros adjusts the beam path length for each image separately, which allows independent focus for each. This greatly minimizes chromatic aberrations, because each wavelength is independently brought into focus. The wavelength of each image is selected using the four interference filters F3 (670 nm), F4 (750 nm), F5 (800 nm), and F6 (900 nm), each of which have a bandpass of 10 nm width. After the images pass through these four filters, they are nearly recombined with beamsplitters BS3 (same

specifications as BS2), and directed to the CCD camera. An image of the sample at each of the four wavelengths is collected in a single frame of the CCD camera.

The camera is a monochromatic CCD chip with 765 x 510 pixels, each 9 μm square. The chip has no anti-blooming, a well capacity of 100,000 e^-, and typical read noise of 13.8 e^-. The chip can be thermoelectrically cooled to ΔT = -40 ˚C, and exposure times range from 0.040 s to 3600 s using a mechanical shutter; in practice the exposure time is usually 0.100 to 5 s. The entire imaging radiometry system is enclosed to minimize stray light.

An example of the image quality in the system is given in Figure 3. The inset shows a reticle as recorded by the imaging radiometry system. For clarity, only the 670 nm image is shown here; the other 3 wavelengths were blocked to avoid overlap with this image. The spacing between lines is 50 μm, and the width of each line is 12.5 μm. Each pixel of the image frame represents a 0.78 μm square point at the sample position. No variation in image magnification with wavelength was measureable; according to the specifications of lenses L1 and L5, image magnification should be constant to <0.05% over the wavelength range of interest. Figure 3 also shows a cross-section across one of the lines on the reticle. If it assumed that the true profile of this line is a step function, then the effective spatial resolution of the imaging radiometry system can be determined by matching the measured profile against a calculated profile in which the step function has been deteriorated by the resolving limit of the system. For this purpose it was assumed that the image deterioration could be described as if it were diffraction limited performance with resolving limit w; the intensity at each point can then be calculated as the following integration of contributions from other points:

$$I_{meas}(a,b) = (C/\lambda)^2 \int\int I_{true} (J_1(q)/q)^2 \, dx \, dy \quad (1)$$

where $q = 3.83 (R/w)$, $R^2 = (x-a)^2+(y-b)^2$, C is a constant, and J_1 is the first-order Bessel function [19]. This calculation is matched to the measured profile in Figure 3, showing that the imaging radiometry system has a spatial resolution of 4.0 μm. The resolving power of the objective lens is nominally 2.0 μm; the practical resolution can probably be improved with further improvement in the other optical components. However, as shown in the Discussion below, the resolving power of the current system introduces only modest artifacts in the measured temperature profiles, and is a significant improvement over earlier methods.

Procedure

Before the laser heating experiments were performed, the four mirrors M3 were adjusted to bring each of the single-wavelength images of the diamond cell sample into focus individually. The positions of the M3 mirrors were then left in place for subsequent measurements, including the calibration, to ensure that the sample was focussed properly in the imaging radiometer whenever it was in focus on camera C1 (Figure 1). The optical response of the imaging radiometry system was calibrated using a 45 W standard lamp, whose irradiance is traceable to NIST standards (Newport Corp. #63358). The lamp was placed behind a 150 μm pinhole that was at the focal plane of the microscope. This pinhole size was chosen because it is small enough that the four images do not overlap on the CCD camera, but it is large enough that Airy diffraction rings near the pinhole edge

do not introduce artifacts in the calibration near the center of the pinhole, where the laser-heating measurements were located. Additionally, any chromatic effects appearing at the edge of the pinhole (which was not focussed through a diamond anvil, as the sample was) were far removed from the location of the laser-heating measurements and do not impact the calibration.

In some experiments, the temperature was measured not only with the imaging radiometry system, but also with a standard spectroradiometric system similar to those described elsewhere [1-6]. This system used a 750 mm f.l. achromat tube lens (Thorlabs AC512-750-B) to produce an image of the laser heated spot onto a 100 μm pinhole aperture. The resulting 19X magnification admitted only thermal emission from the central 5.3 μm of the laser heated spot. This light was then focussed into a 0.3 m spectrograph (PI Acton SpectraPro SP-2356) and detected with a digital CCD camera (PI Acton PIXIS 100F). The standard spectroradiometry system was calibrated in a similar way as the multispectral imaging radiometer, using the same lamp and pinhole aperture. The thermal emission spectrum from 630 nm to 930 nm was used to calculate temperatures.

During the laser heating experiments, the sample was viewed with both the analog camera (C1, Figure 1) and the CCD detector (C2, Figure 2). The laser power was increased until the sample emission reached the desired level, then a frame from C2 was captured. In some experiments, a spectrum was collected at the same time using the standard spectroradiometer (Figure 1). After data collection, either the laser was turned off, or data collection continued at the same or a different laser power. Background frames were collected both before and after data collection.

DATA ANALYSIS

A representative data image is shown in Figure 4. The laser heated spot is recorded at each of the four wavelengths simultaneously. There are several steps to the data analysis procedure that converts images like these to temperature maps of the hot spot: background subtraction, intensity calibration, spatial correlation of the four image spots, and temperature calculation.

Background subtraction

There are three sources of background to the recorded image: detector noise, stray light from sources other than the laser heated spot, and scattered light from the hot spot that has been rejected by the interference filters but remains inside the imaging radiometry enclosure. Proper background subtraction is essential to measure large temperature gradients [9].

Detector noise includes dark and readout noise, and is easily removed. This source of background is very repeatable as long as the detector temperature remains constant. We normally set the thermoelectric cooling setpoint of the SBIG ST-402ME camera to –10 ˚C, which reduces the detector noise significantly. The camera is usually also set to automatically subtract a dark frame, which is obtained by collecting a frame with the shutter closed, using the same exposure time as the sample frame.

Stray light, from sources (on the optical bench or elsewhere in the room) other than the laser heated spot, has been kept to a minimum by a series of enclosures. First, the entire optical table is covered in an aluminum box that reduces dust and light but has removable panels for access. Second, on the optical table the imaging radiometry system is enclosed from the other optics by a set of black fabric curtains that are sealed with black tape. Light from the optical table is only permitted through a 25 mm diameter x 300 mm tube that projects through the curtain (Figure 2). With these precautions, external stray light has been reduced to negligible levels. Nevertheless, a background frame, taken with the laser off but otherwise identical operating conditions as the sample frame, is subtracted from the sample frame.

The most persistent source of background light in the measurement is a flatfield background that is produced by scattered light within the imaging radiometry system. Although a broadband source, from 600 nm to 950 nm, is introduced into the system, only four wavelength bands, with a bandpass 10 nm wide each, are transmitted completely through the system onto the CCD. Furthermore, even at these selected bands the transmission of the apparatus is low, <1%, because of the numerous (5 or 6) passes through the beamsplitters in addition to losses at the interference filters and other optical elements. The rejected light scatters inside the enclosure; some of that light reaches the CCD. This scattered light produces a flat (approximately) background level that is typically ~1% of the peak intensity in the image. This background is measured in a region that does not overlap the hot spot images, and removed as a uniform level from the entire frame. It is this background, and not the camera characteristics, that ultimately limits the useful dynamic range of the measurement, and consequently limits the range of

temperatures that can be measured from a single image. The uncertainties introduced by background subtraction are easily seen in the misfits to the thermal emission spectrum in outer regions of the hot spot (see below). Future improvement of the system may focus on reducing this background.

Intensity calibration

Intensities are calibrated to a standard lamp with known irradiance, as described in the Experimental section. The pinhole aperture used in the calibration was chosen with a 150 μm diameter because this size is large enough that Airy diffraction rings do not appear in the central region where the hot spot image will appear, but small enough that the four single-wavelength images of the pinhole do not overlap on the CCD detector. After background subtraction for both, the sample frame is divided by the calibration frame to form a lamp-corrected frame. At this point the lamp-corrected frame has not yet been corrected for the known irradiance of the lamp, because the frame still contains images from more than one wavelength .

Spatial correlation

The lamp-corrected frame must now be separated into four different subframes, each containing a single-wavelength image of the hot spot. Usually a set of 50 x 50 pixel subframes was more than sufficient to capture the useful information from each hot spot. It is important that these images were precisely correlated spatially, to allow point-to-point comparisons of pixel intensities so the temperature map of the hot spot was accurately calculated. Best results for spatial correlation of the four subframes usually

were achieved by analyzing a frame taken from the laser heated sample itself. An image of the sample recorded using reflected or transmitted light could be used for this purpose, and matching the peak intensities from the four laser-heated spot images worked especially well. Interpolations between pixels were performed to attain the closest spatial correlation possible.

One subframe (the 750 nm image subframe) was chosen as a set of 50x50 pixels encompassing the hot spot and then held fixed. The other 3 subframes (650 nm, 800 nm, and 900 nm images) were assigned XY offsets (numbers of pixels) relative to the 750 nm subframe; these offsets were tuned to achieve optimum subimage mapping. The tuning of the offsets was performed by examining horizontal (X) and vertical (Y) intensity profiles across a recognizable feature in the image, and selecting the offset values that brought these profiles into coincidence. An appropriate feature for this purpose could be a small grain recorded in transmitted light, or even the laser heated spot itself (maximum intensities should coincide at each wavelength). Interpolations were performed by weighted averages between neighboring pixels. In practice one could usually bring all 4 subframes into coincidence within 0.1 pixels (i.e., 0.08 μm).

Temperature map calculation

At this stage of the data analysis, each of the four subframes contained a single wavelength, lamp-corrected image. These subframes were each multiplied by the known irradiance of the standard lamp at their respective wavelengths; the polynomial provided by the lamp's calibration was used for these irradiances. At each spatially correlated pixel

position, the four calibrated intensities were fitted to the Planck radiation function to calculate the temperature of the sample at that point:

$$I = c_1 \varepsilon \lambda^{-5} / (\exp(c_2/\lambda T)-1) \quad (2)$$

where I is the intensity of emission, ε is the sample emissivity, λ is wavelength, and T is temperature. The constant c_1 contains fundamental physical constants and geometrical factors specific to the experiment, and the constant c_2 is hc/k. The graybody approximation, in which the sample emissivity (ε) is assumed to be independent of wavelength, was used as is normally the case in this application [1]. For convenience, the Wien approximation can be used to simplify the data processing; this introduces negligible error below 4000 K [1].

RESULTS and DISCUSSION

Melting of Pt at 1 bar

The accuracy of the method can be evaluated by using it to measure a well known fixed point, like the melting point of platinum at 1 bar. Platinum was chosen for this test because it absorbs the laser readily, it melts congruently, and is highly resistant to oxidation; platinum group elements remain metallic when heated to their melting point even in air.

A platinum foil, 0.025 mm thick, was secured to an aluminum block and laser heated on one side. At high temperature, the multispectral imaging radiometry system was used to measure the temperature distribution of the laser heated spot, which was approximately 35 μm across. The result is shown in Figure 5. The temperature distribution in this hot spot is radial but not perfectly symmetrical, as is frequently assumed for calculated gradients in laser heated spots. The temperature gradient is measureable from a peak of 2440 K down to approximately 1850 K, limited by the signal to background ratio in the recorded image frame.

The temperature range spanned by the laser heated spot encompasses the melting point of Pt, 2045 K. The melting point can be identified in the temperature map data by a discontinuity in the temperature-emissivity profiles across the hot spot, because the emissivity is a material property of the sample that changes upon melting. This is demonstrated in Figure 6, in which a sharp discontinuity is observed at 2049 K in the temperature-emissivity data along a profile across the peak of the hot spot that was shown in Figure 5. By examining different profiles across the hot spot, and set of emissivity discontinuities can be identified, each related to the appearance of melt in the hot spot. Examination of 21 such profiles generated a mean and standard deviation of 2039±42 K, in good agreement with the known melting point (2045 K). This test of multispectral imaging radiometry compares well with similar tests performed with earlier methods of laser heating temperature measurement[1,4].

Heating of Fe at 20 GPa, and comparison to spectroradiometry

Additional tests of the method, and direct comparison to the standard spectroradiometric system, were made by heating an Fe foil at 20 GPa in a diamond anvil cell. A typical temperature map of the Fe sample in the laser heated diamond anvil cell is presented in Figure 5b. In the following experiments, both multispectral imaging radiometry and spectroradiometry were used simultaneously to measure the temperature of the laser heated spot.

In the first of these tests, the laser power was increased gradually, with temperature measurements taken at each power step. This permitted a comparison of the two systems with the spectroradiometer aligned with the central 5.3 μm of the laser heated spot. These spectroradiometrically measured temperatures are compared in Figure 7 to the temperatures calculated from an equivalent region of the four single-wavelength images in the imaging radiometry system.

In a second test, the laser beam was moved, so the 5.3 μm diameter area that was measured by the spectroradiometer was off of the hot spot peak, where the gradients are greater. Again, for comparison, the equivalent region was averaged for temperature measurement by multispectral imaging radiometry. A series of adjustments to the laser position allowed various points along the temperature gradient to be measured. These results show an equivalent comparison between the two methods as was obtained from the on-peak measurements (Figure 7).

In both tests, the measured temperatures are strongly correlated, but the spectroradiometric temperature is systematically higher by an average of approximately 30 K (Figure 7). The source of this offset is unknown, but it seems possible that, despite

careful alignment and calibration, when using refractive optics (plus the diamond anvil) the chromatic effects at the pinhole aperture cannot be perfectly corrected in the standard spectroradiometer. However, in practical terms this is an acceptable level of agreement between laser heating temperature measurement systems. Interlaboratory comparisons of laser heated diamond anvil studies are rarely in agreement to better than 100 K.

Error analysis of 4-color method

The first two tests of the multispectral imaging radiometry system, against the melting of Pt at 1 bar and against the standard spectroradiometric method in a diamond anvil cell, were ways to gauge the accuracy of the method. One must also consider its precision, particularly the loss of precision that can be expected in a 4-color temperature measurement compared to the hundreds or more channels commonly used in spectroradiometry.

One measure of precision for standard spectroradiometry is the error in the fit to the Planck function. Because of the large numbers of channels in the spectrum, the statistical fit to the Planck function is usually quite small. For example, the statistical fit to the spectroradiometric data presented in Figure 7 are on the order of 5 K. However, this is only an internal precision; tests of laser heating temperature measurement systems against melting of elements at 1 bar typically report reproduceabilities of 50 K or worse [1,4]. Therefore, the precision provided by the large number of wavelengths in the spectrum is not necessary to the method. As seen in Figures 6 and 7, the precision on temperature from the 4-color fits in the imaging radiometry ranges from 10 to 70 K, comparable to the accuracy estimated from the Pt melting experiments above.

Analysis of image correlation

As discussed in the Experimental section, the spatial correlation of the 4 spectral subframes is a critical part of the data analysis procedure. It is important to evaluate the effects that one could encounter if there were misalignments between these image subframes. To demonstrate these effects, one can use the data from the earlier example of laser heating Fe in the diamond anvil cell (Figures 4b and 5b); this is a sensitive test because that hot spot is relatively small, so the gradients in image intensity are large.

Figure 8a shows a temperature profile across the laser heated spot from Figure 5b. The corresponding emissivity-temperature plot from this profile, analogous to that used to identify Pt melting in Figure 6, is presented in Figure 8b. To demonstrate the effect of a misalignment between the spectral subframes used to generate these data, the 900 nm subframe was deliberately shifted by 0.5 μm; the resulting temperature profile and emissivity-temperature plots are shown in Figure 8 for comparison to the properly correlated data.

When the subframes were all aligned, the temperature profile was peaked in the center, as expected (Figure 8a), and the position of the peak temperature was coincident with the peak intensity. This sample contained no phase changes, so the emissivity was not a strong function of temperature (Figure 8b). The deliberate misalignment of the 900 nm subframe had a noticeable effect on the temperature distribution. On the left side of the temperature profile, the 900 nm intensity increased, so the calculated temperatures were lower; on the right side of the profile the converse was true (Figure 8a). The error introduced by this misalignment was ~70 K, but smaller near the peak. It should be

emphasized that misalignment of the 900 nm subframe by 0.5 μm is unlikely in practice; coalignment of all 4 subframes to within 0.1 μm is more typical.

In the event that misalignment of the spectral subframes were to occur, there are indicators that could reveal to the user that this has happened. First, the position of the peak calculated temperature is shifted (Figure 8a), and will not coincide with the maximum intensity of the image; this is unphysical in most cases. Second, the emissivity-temperature (ε-T) plot provides a strong indication of misalignment, shown in Figure 8b. When the four subframes are properly aligned, the ε-T relationship is practically the same on both halves of the profile. However, when the subframes are not properly coaligned, the ε-T relationship is noticeably different on either side of the profile. This occurs because the relative emissivity, obtained as a fitting parameter to the Planck function, is more sensitive to misalignment of the images than the temperature is. Consequently, these two indicators, that are internal to the data analysis (Figure 8), can signal the presence of spatial misalignment during the image processing. Attention should be paid to these indicators to maintain quality in the data processing for imaging radiometry measurements.

Effect of spatial resolution

A concern with any measurement of laser heated spots is the effect that limited spatial resolution has on the measured temperature. It is important to consider the consequences of the resolving power of the imaging radiometry system (4.0 μm at 670 nm; Figure 3). Figure 9 presents a calculation illustrating the impact of this resolving power on the measurement. The temperature distribution in this example was chosen to

be Gaussian with a characteristic radius of 15 μm, similar to the intensity profile of the incident laser in the laser heating system described in Figure 1. From this assumed temperature distribution, a set of intensity distributions at 670 nm, 750 nm, 800 nm, and 900 nm were calculated from Planck's radiation function. From each of these single-wavelength 2-D distributions, an "blurred" distribution was calculated based on the loss of spatial resolution from the limits of resolving power of the optical system. The procedure was analogous to that used to evaluate the spatial resolution in Figure 3; equation 1 was used to represent the resolving power's effect. (Note also that the spatial resolution is proportional to wavelength; $w = w_{670}(\lambda/670)$. [19]) Then each point in the blurred intensity distributions was fit to Planck's curve to generate a 4-color temperature, similar to the way in which a real measurement is processed.

This blurred distribution is compared to the input temperature distribution in Figure 9. The increase in peak temperature is principally a consequence of the fact that spatial resolution at long wavelengths is poorer than at shorter wavelengths, so the peak loses infrared light preferentially over red light, which increases the apparent temperature. The apparent temperatures at positions far from the peak also increase, but for a different reason; here, the measured signal is contaminated more by blurring from the intense high-T neighboring region (at low radii) than it is by blurring from the less intense low-T neighboring region (at higher radii). Regardless, the blurring effect with this level of resolving power is not very large, only 30 to 60 K across the central 20 μm diameter region of the hot spot. However, at points far from the peak, the error becomes significantly greater; for example, at a radius of 14 μm the misfit reaches 130 K in Figure 9. Additional calculations show that these differences between the true and apparent

temperature do not change much as the peak temperature is varied, and can be greatly reduced by increasing the laser beam diameter.

The effect of spatial resolution on measured temperature profiles from laser heated spots is not confined to the imaging radiometry system described here. It applies to all laser heating systems, whether the gradients are measured explicitly or the aperture method is used to measure only a central temperature. Of course the magnitude of the effect depends strongly on the resolving power of the system. However, the true spatial resolution of temperature measurement systems for laser heating is often not reported, in part because it is less straightforward to quantify the resolving power in non-imaging systems.

CONCLUSIONS

A multispectral imaging radiometry system has been described that measures the temperature distribution in laser heated diamond anvil samples. The method is not specific to laser heating nor to diamond anvil cell samples, and can be applied to measuring temperature distributions of any hot spot with suitable adaptation of the delivery optics that transmit the sample image into the system. The method is also easily adaptable to a greater number of wavelengths, although there is a tradeoff between number of wavelengths and transmitted intensity.

There are several significant advantages of multispectral imaging radiometry over earlier methods of temperature measurement in the laser heated diamond anvil cell:

1. Two-dimensional maps of temperature and emissivity across the hot spot are both obtained. Knowledge of the temperature distribution is essential to proper interpretation of other measurements that may be obtained from the sample, such as x-ray diffraction measurements or chemical microanalysis by electron microscopy. Furthermore, determining the temperature without assuming that the emissivity is constant across the hot spot makes the measurement much more robust, not only when measuring a single phase sample, but especially when there may be a phase transition within the hot spot. In addition, phase changes can sometimes be recognized by a discontinuity in the temperature-emissivity relationship (Figure 6).

2. Chromatic aberrations are avoided because each wavelength is focussed independently. All polychromatic images obtained from a diamond anvil cell bear chromatic aberrations because of the high dispersion of diamond, and usually other elements in the optical path too (e.g., microscope objectives, beamsplitters). These chromatic aberrations have been the source of much consternation around temperature measurement of laser heated spots, because the pinhole or slit apertures (or pixel rows) that select portions of the image necessarily behave differently at different wavelengths [4,5,10,13]. A key advantage of the multispectral imaging radiometry system described here is that it frees the laser heating system from these concerns. Not only does this provide a more accurate temperature measurement, it also permits the experimenter to make different design decisions in other aspects of the laser heating system, without concern for the chromatism that might be introduced.

3. All single-wavelength images are obtained simultaneously. Temperature distributions in laser heated diamond cell samples are often not constant with time,

especially in the important circumstance of a sample undergoing a phase transition. It is essential that temperature calculations be performed on images that were obtained simultaneously to avoid significant errors due to temporal variations in intensity.

Some weaknesses persist in the current design, but these are relatively minor. Better rejection of scattered light from the multispectral image (Figure 4) could lead to improved signal-to-background, thus expanding the temperature range over which each hot spot can be measured (Figure 5). However, with finite spatial resolution there is a limit to the temperature range that can be measured accurately (Figure 9). Further improvements in image quality will slightly enhance the accuracy of the temperature maps, but as discussed above the current design is satisfactory given other limitations of the laser heating method.

ACKNOWLEDGMENTS

I am grateful to A. Kavner, for discussions and for a preprint of her recent work, and also to S. Clark, for a thoughtful review. This project was supported in part by NSF grant EAR-0635722.

REFERENCES

[1]Heinz D. L. and R. Jeanloz, in *High-Pressure Research in Mineral Physics*, edited by M. H. Manghnani and Y. Syono (American Geophysical Union, Washington, DC, 1987).

[2]R. Boehler, N. von Bargen, and A. Chopelas, J. Geophys. Res. **95**, 21731 (1990).

[3]P. Lazor, G. Shen, and S. K. Saxena, Phys. Chem. Minerals **20**, 86 (1993).

[4]G. Shen, M. L. Rivers, Y. B. Wang, and S. R. Sutton, Rev. Sci. Instrum. **72**, 1273 (2001).

[5]M. J. Walter and K. T. Koga, Phys. Earth Planet. Int. **143-144**, 541 (2004).

[6]T. Watanuki, O. Shimomura, T. Yagi, T. Kondo, and M. Isshiki, Rev. Sci. Instrum. **72**, 1289.

[7]R. Jeanloz and A. Kavner, Phil. Trans. R. Soc. Lond. A **354**, 1279 (1996).

[8]A. Kavner and R. Jeanloz, J. Appl. Phys. **83**, 7553 (1998).

[9]A. Kavner and W. R. Panero, Phys. Earth Planet. Int. **143-144**, 527 (2004).

[10]J. S. Sweeney and D. L. Heinz, in *Properties of Earth and Planetary Materials at High Pressure and Temperature*, edited by M. H. Manghnani and T. Yagi (American Geophysical Union, Washington, DC, 1998).

[11]R. Boehler, Rev. Geophys. **38**, 221 (2000).

[12]Q. Williams, E. Knittle, and R. Jeanloz, J. Geophys. Res. **96**, 2171 (1991).

[13]L. R. Benedetti, N. Guignot, and D. L. Farber, J. Appl. Phys. **101**, 013109 (2007).

[14]G. A. Lyzenga and T. J. Ahrens, Rev. Sci. Instrum. **50**, 1421 (1979).

[15]M. B. Boslough and T. J. Ahrens, Rev. Sci. Instrum. **60**, 3711 (1989).

[16]K. G. Holland and T. J. Ahrens, Science **275**, 1623 (1997).

[17]A. Kavner and C. Nugent, Rev. Sci. Instrum. (submitted).

[18]H. K. Mao, P. M. Bell, J. W. Shaner, and D. J. Steinberg, J. Appl. Phys. **49**, 3276 (1978).

[19]K. D. Möller, *Optics* (University Science Books, Mill Valley, CA, 1988).

FIGURE CAPTIONS

Figure 1. Laser heating system. DAC: Diamond anvil cell, symmetric-type, Princeton University. LASER: 50 W fiber laser, 1064 nm, polarized, IGP Photonics YLP-50-1064-LP. L1: NIR 5X objective lens, Mitutoyo 378-822. L2: Achromat concave lens, -51.5 mm at 1064 nm, CVI Laser PCB-25.4-51.5-C-1064. L3: Achromat convex lens, 65.4 mm at 1064 nm, CVI Laser PXB-25.4-65.4-C-1064. L4: Achromat NIR lens, 200 mm, Thorlabs AC254-200-B. M1: Laser mirror, 1064 nm, Newport 10QM20HM.15. BS1: Pellicle beamsplitter, 700-900 nm coating, Thorlabs BP145B2. C1: CCD observation camera, Hitachi KP-D20A. F1: 950 nm short pass filter, Thorlabs FES0950. F2: red dichroic filter, Thorlabs FD1R. Not shown in this figure are additional optics that allow double sided laser heating by splitting the laser beam and focussing it onto both sides of the sample; this feature was not used for the experiments described here.

Figure 2. (Color online) Multispectral imaging radiometry system. The beamsplitters and interference filters split the incoming light into four spectral bands, which are focussed as separate images and recorded simultaneously by the CCD detector. L5: Achromat NIR lens, 500 mm, Thorlabs AC254-500-B. M2 and M3: Silver mirror, Thorlabs PF10-03-P01. BS2 and BS3: Low-polarizing cube beamsplitters, coated for 600-900 nm, OptoSigma 039-0265. F3: 670 nm interference filter, OptoSigma 079-1490. F4: 750 nm interference filter, OptoSigma 079-1590. F5: 800 nm interference filter, OptoSigma 079-1780. F6: 900 nm interference filter, OptoSigma 079-2770. C2: CCD detector, SBIG ST-

402ME. The four M3 mirrors are mounted on separate translation stages, that permit independent focussing of each of the four narrow-bandpass images.

Figure 3. Evaluation of spatial resolution of imaging radiometry system. Inset: Image of a reticle recorded by the imaging radiometry system. Only the 670 nm wavelength image is shown; the other 3 wavelengths were blocked to avoid overlap. The spacing between lines is 50 μm, and the line width is 12.5 μm. Plot: Measured intensity profile (crosses) across a reticle line from the inset picture, compared to a calculated profile (open circles) using a resolving power of 4.0 μm. See text for details.

Figure 4. Multispectral imaging of laser heated spots using the imaging radiometry system. Each strip is from a single CCD camera frame, and contains four single-wavelength images, from left to right: 670 nm, 750 nm, 800 nm, 900 nm. Calibration of these frames permits temperatures to be calculated at each pixel. a) Platinum foil at 1 bar. b) Iron in a diamond anvil cell at 20 GPa.

Figure 5. (Color online) Temperature maps of laser heated spots, measured using multispectral imaging radiometry. Calibration bars labelled in Kelvin. a) Platinum foil at 1 bar, shown in Figure 4a. The map is 40 μm across, and each line represents a row of 0.78 μm square pixels. b) Iron in a diamond anvil cell at 20 GPa, shown in Figure 4b. The map is 24 μm across, and each line represents a row of 0.78 μm square pixels.

Figure 6. Temperature vs. emissivity plot along a peak-to-rim transect of the Pt hot spot in Figure 5a. The sharp discontinuity at 2049 K is associated with melting.

Figure 7. Comparison of temperatures measured by standard spectroradiometry vs. multispectral imaging radiometry. Temperatures were made simultaneously from the same laser heated spot, on iron in a diamond anvil cell at 20 GPa. Circles: measurements made at center of laser heated spot, varying laser power. Squares: measurements made along the gradient of a laser heated spot, at fixed laser power but moving laser beam.

Figure 8. Effect of misalignment of spectral images on the calculated temperature distribution. Solid circles: temperatures across laser heated spot shown in Figures 4b and 5b, with spectral images in correct spatial coalignment. Open circles: temperatures obtained from the same raw data, with the 900 nm image deliberately misaligned by 0.5 μm. a) Temperature profile. b) Emissivity vs. Temperature plot. The disturbance in the ε-T relationship is a symptom of misalignment of the spectral images.

Figure 9. Effect of spatial resolution on measured temperature distribution from a laser heated spot. The input distribution (dashed curve) assumed a Gaussian profile with a radius of 15 μm, a peak temperature of 2500 K, and a background of 300 K. The apparent temperature distribution (squares) was modelled to illustrate the effect of a resolving power of 4.0 μm at 670 nm (Figure 3). Measured graybody temperatures overestimate the true temperature by only 30-60 K over the central 20 μm of the hotspot. See text for details.

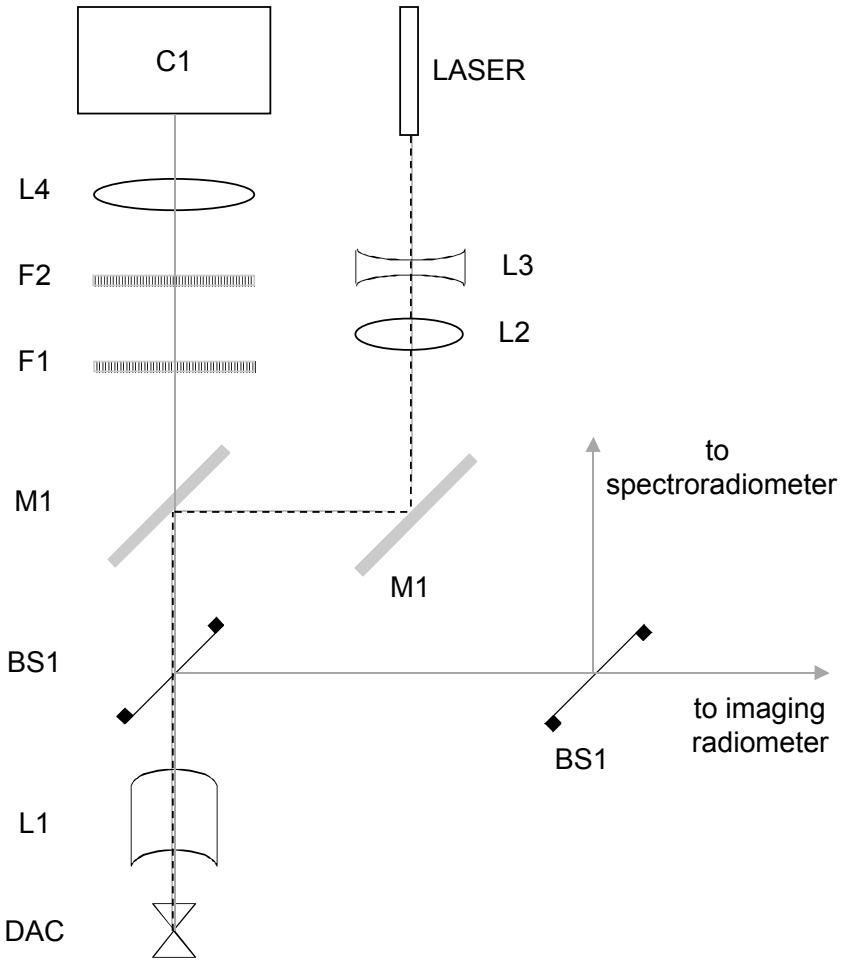
C1
LASER
L4
F2
L3
F1
L2
M1
to
spectroradiometer
M1
BS1
to imaging
radiometer
BS1
L1
DAC

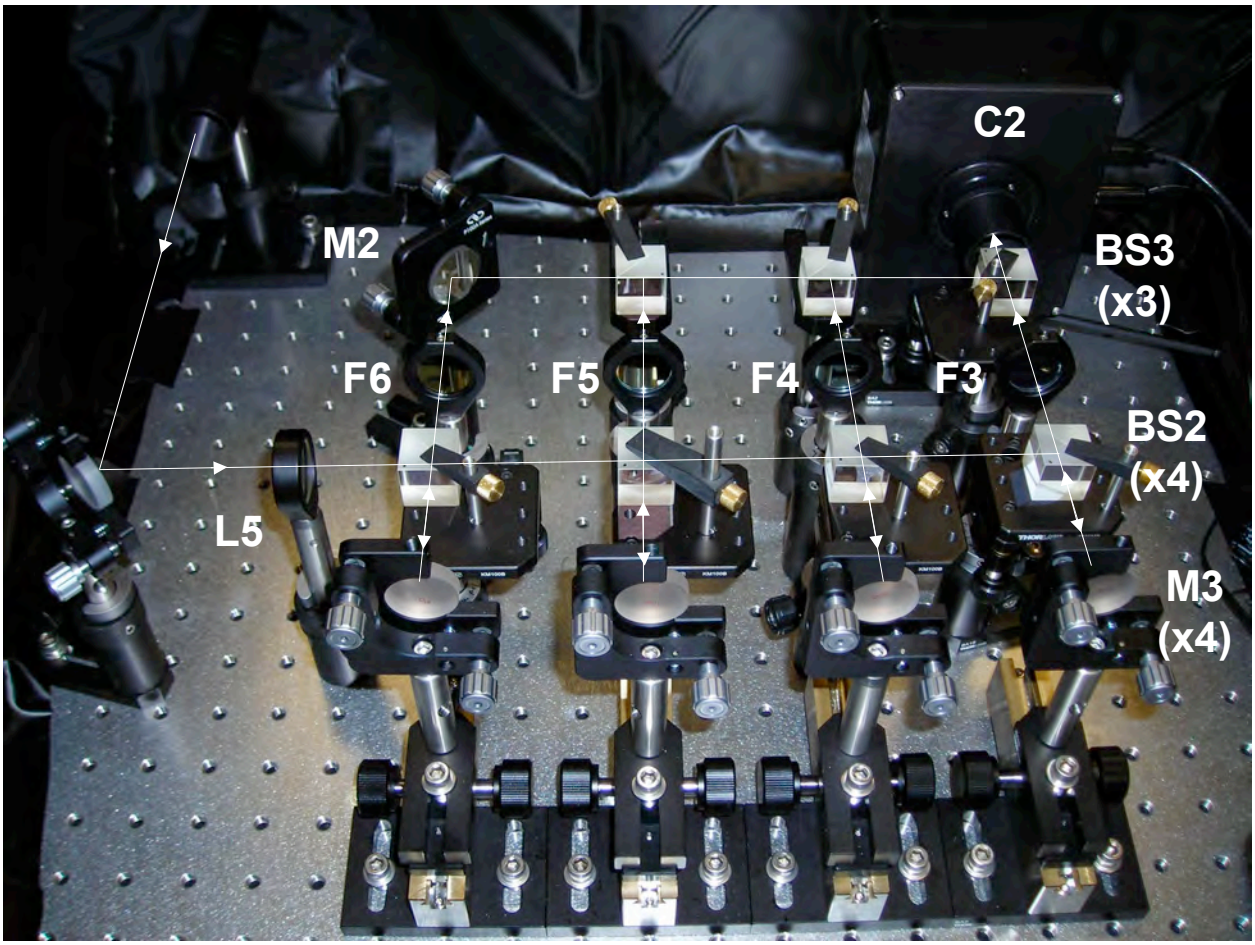
C2
M2
BS3
(x3)
F6
F5
F4
F3
BS2
(x4)
L5
M3
(x4)

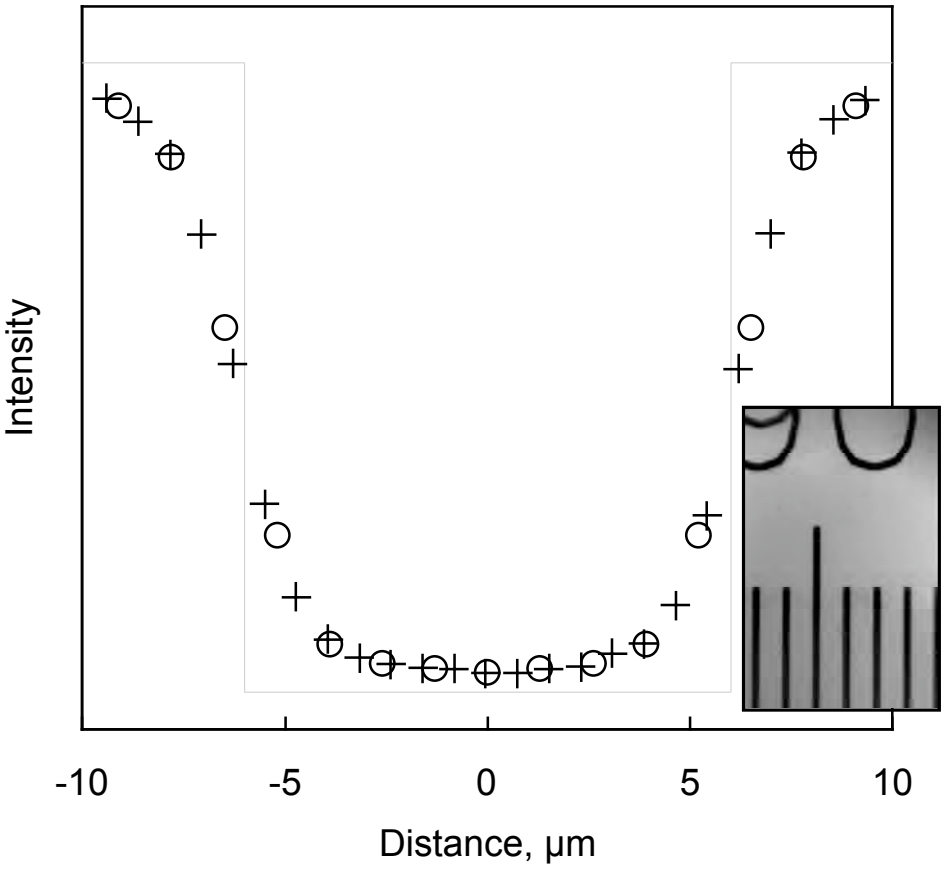
Intensity
-10
-5
0
5
10
Distance, μm

a

b

a

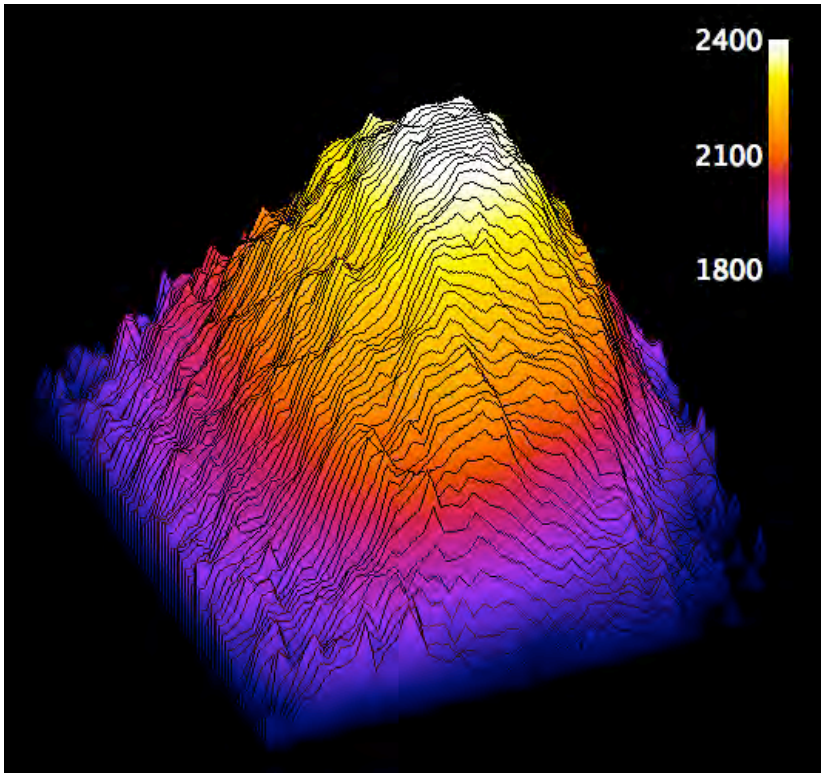

b

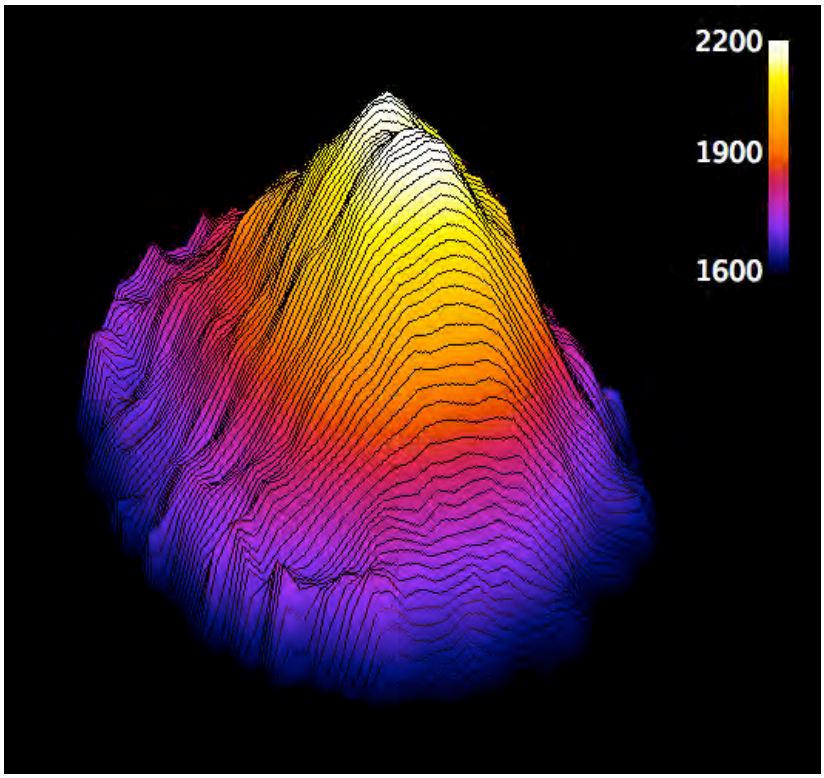

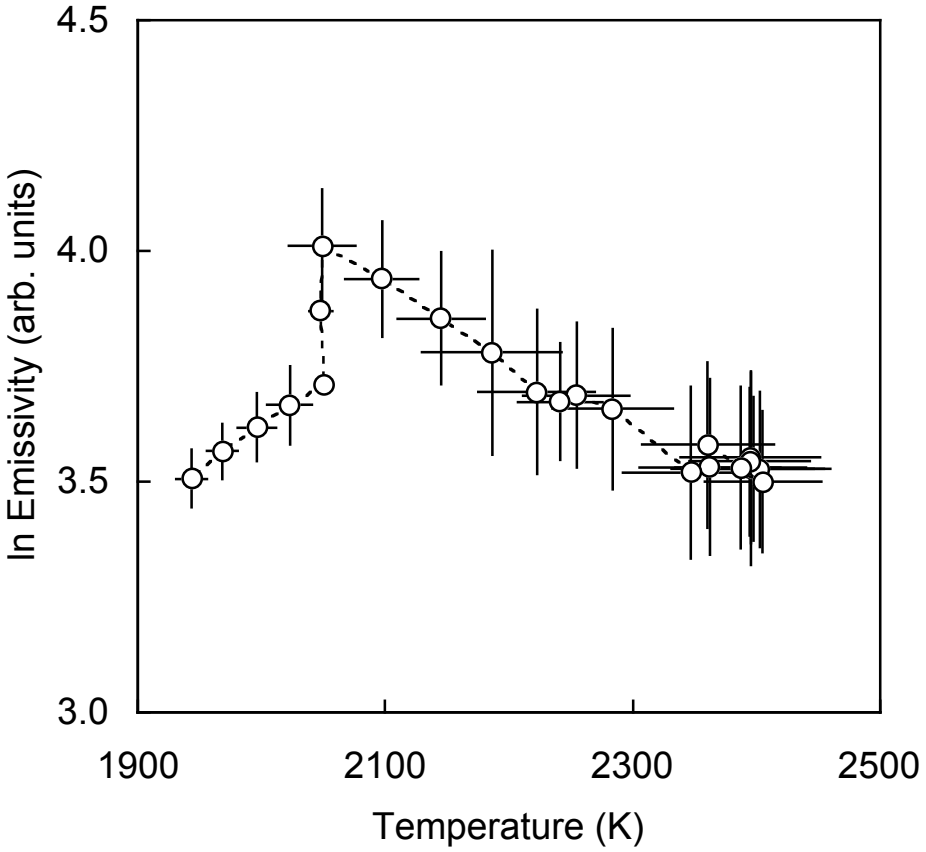
4.5
4.0
3.5
3.0
ln Emissivity (arb. units)
1900
2100
2300
2500
Temperature (K)

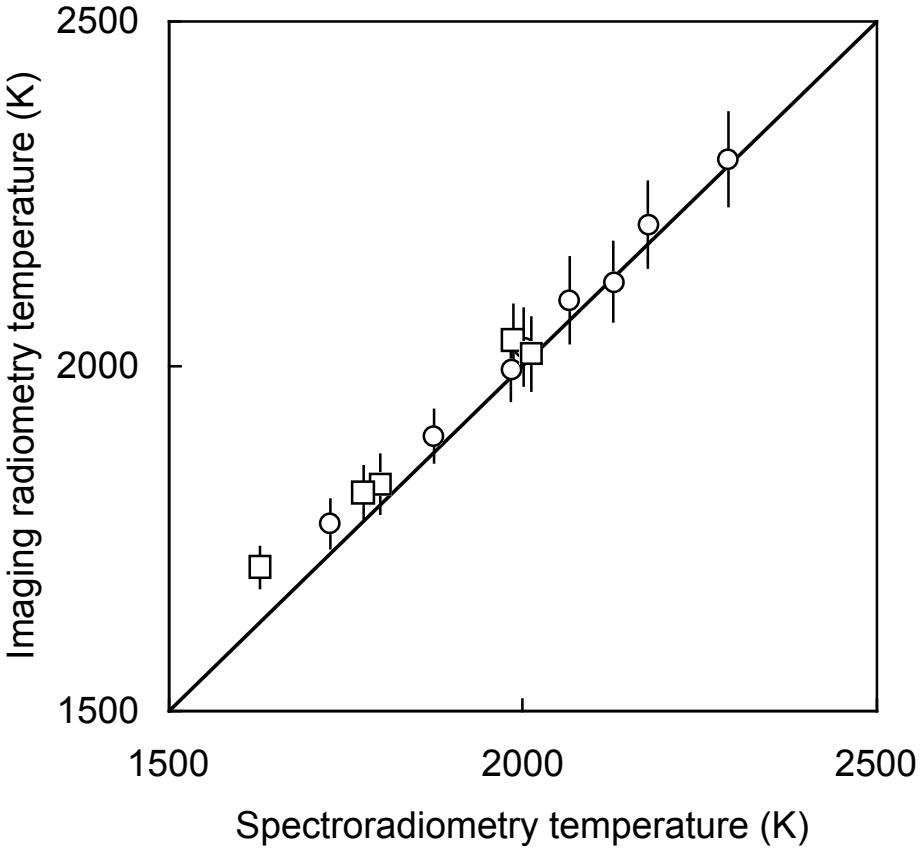
2500
2000
1500
Imaging radiometry temperature (K)
1500
2000
2500
Spectroradiometry temperature (K)

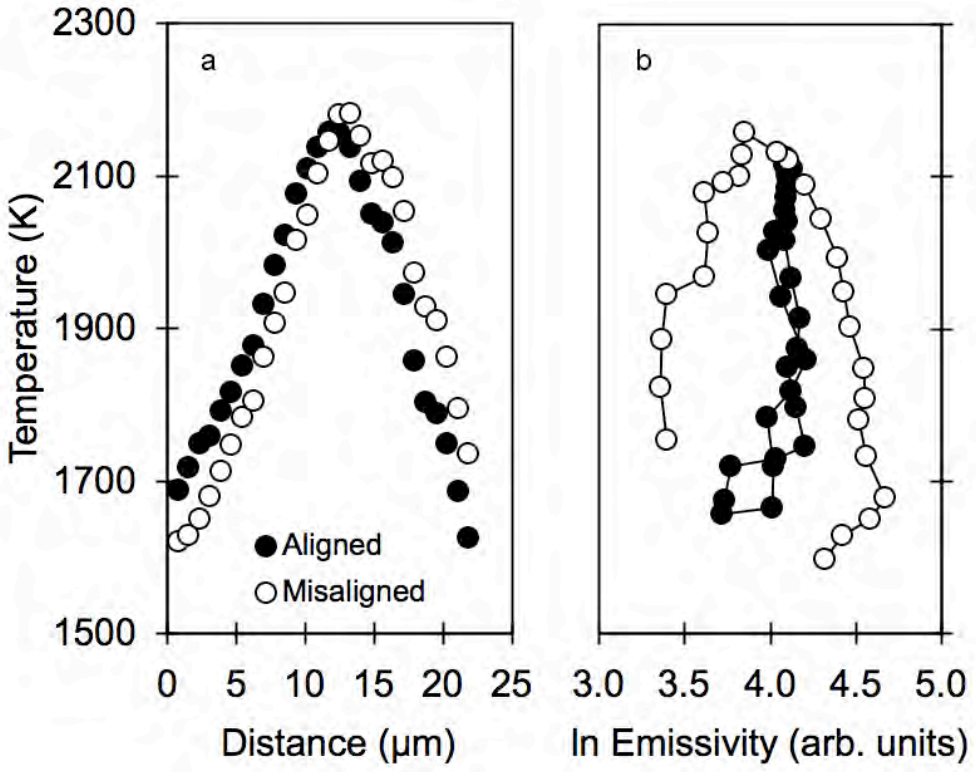
a
b
2300
2100
1900
1700
1500
Temperature (K)
Aligned
Misaligned
0
5
10
15
20
25
Distance (μm)
3.0
3.5
4.0
4.5
5.0
ln Emissivity (arb. units)

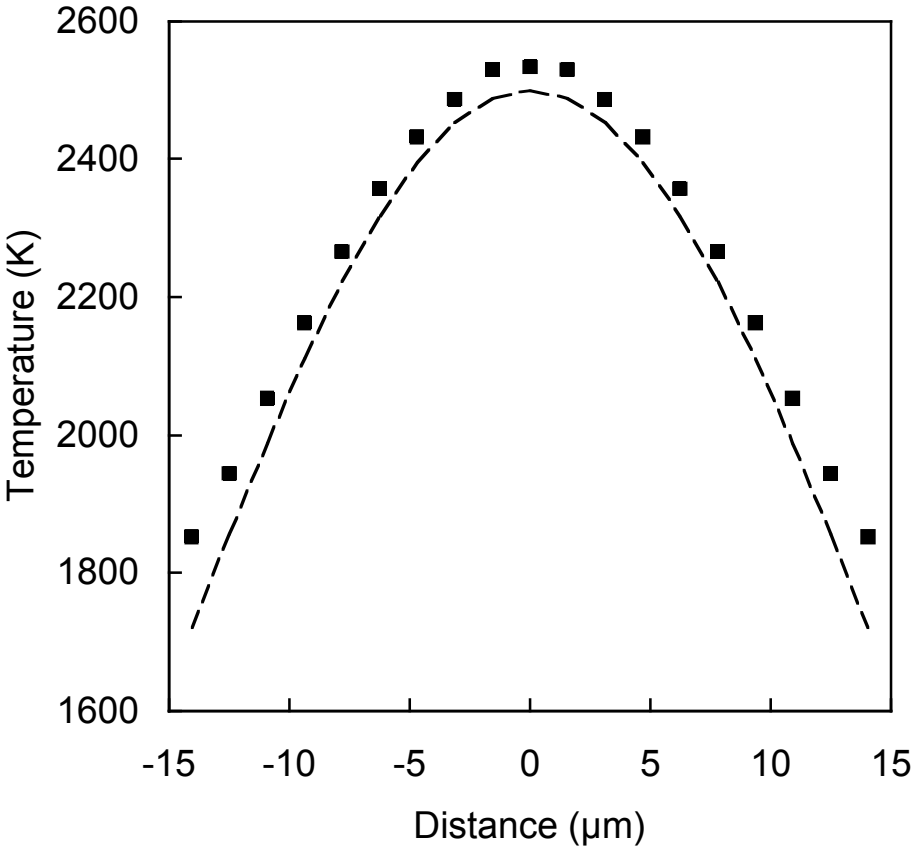
2600
2400
2200
2000
1800
1600
Temperature (K)
-15
-10
-5
0
5
10
15
Distance (μm)